Microfluid Nanofluid (2010) 9:267–280
DOI 10.1007/s10404-009-0544-0

RESEARCH PAPER

A multifunction and bidirectional valve-less rectification micropump based on bifurcation geometry

Ahmed Fadl · Stefanie Demming · Zongqin Zhang · Stephanus Büttgenbach · Mannfred Krafczyk · Donna M. L. Meyer

Received: 24 September 2009 / Accepted: 26 November 2009 / Published online: 24 December 2009

Abstract In this paper, we introduce a novel valve-less rectification micropump based on bifurcation geometry. Three micropumps based on three different bifurcation configurations were designed, fabricated and experimentally investigated. These designs demonstrate the potentials of developing bidirectional micropumps and multifunction microfluidic devices (combined functions of micro pumping and mixing). Polydimethylsiloxane (PDMS) was employed to fabricate the micropumps. Circular piezoelectric transducers (PZT) were used as flow actuators. Detailed fabrication procedures are illustrated. The micropumps were tested against two ranges of actuator frequencies. The first test was conducted in a frequency range between 0 and 100 Hz with small increments of 5 Hz, while the second test was conducted in a frequency range between 0 and 300 Hz with increments of 50 Hz. Ethanol was used as the working fluid in all experiments. A new dimensionless parameter was introduced to evaluate the efficiency of valve-less rectification micropumps and determine the optimum operational frequency. The flow rate and maximum back pressure were measured. Results of experiments confirmed and demonstrated the feasibility of valve-less rectification micropumps based on bifurcation geometry at a low frequency range. Additionally, results showed the potentials of multifunctional, bidirectional, and self-priming micropumps.

Keywords Valve-less rectification micropumps · Microfluidic diodicity · Bifurcation · Rectifying geometries

A. Fadl (✉) · Z. Zhang · D. M. L. Meyer
Department of Mechanical Engineering and Applied Mechanics, University of Rhode Island, Kingston, RI, USA
e-mail: fadla@egr.uri.edu

A. Fadl · M. Krafczyk
Institute of Computational Modeling in Civil Engineering, Technical University of Braunschweig, Braunschweig, Germany

A. Fadl · S. Demming · S. Büttgenbach
Institute of Microtechnology, Technical University of Braunschweig, Braunschweig, Germany

1 Introduction

Many studies on developing, modeling and optimization of micropumps have been published in the past decade (Nguyen et al. 2002; Laser and Santiago 2004; Iverson and Garimella 2008; Amirouche et al. 2009). Micropumps can be categorized with respect to their working principles as mechanical and non-mechanical micropumps. Mechanical micropumps usually use mechanical parts to deliver a constant fluid volume. Examples of mechanical micropumps are rotary, peristaltic, check valves, and valve-less rectification micropumps. The valve-less rectification micropump can be further categorized as a displacement mechanical micropump. On the other hand, non-mechanical micropumps add momentum to the fluid by converting another energy form into kinetic energy. Examples of non-mechanical micropumps are electrokinetic, magnetohydrodynamic, and electrochemical micropumps.

The valve-less rectification micropumps have gained increased research attentions in recent years. The advantages of valve-less rectification micropumps include having no-moving parts, ease to fabricate, cost effective, having the ability to pump particle-laden fluids and live cells, being compatible with a wide range of materials and working fluids, and delivering a favorable flow rate and back pressure (Stemme and Stemme 1993; Olsson et al. 2000; Yamahata et al. 2005). Figure 1 shows the working

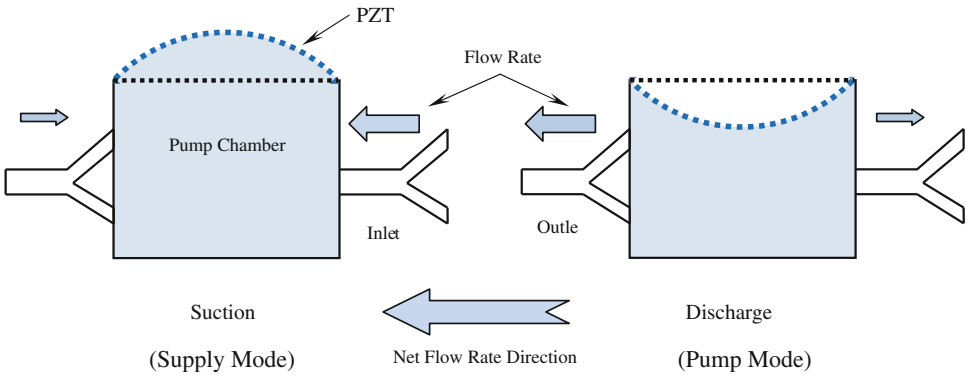

Fig. 1 The pumping mechanism of the valve-less rectification micropump

principles of the valve-less rectification micropump. In the supply mode, the piezoelectric transducers (PZT) diaphragm moves upward and generates a negative pressure inside the pump chamber. As a result, the fluid flows into the chamber. More fluid enters from the right bifurcation compared with the left one due to the difference in the flow resistance. On the other hand, when the PZT moves downward, in the pump mode, a positive pressure is generated inside the pump chamber. Therefore, the fluid flows out of the chamber. More fluid exits the left bifurcation compared with the right one during the pump mode. Due to the combined effects of the PZT diaphragm oscillation, a net flow rate is observed from the direction of right to left.

The efficiency of the valve-less rectification micropump depends primarily on the microfluidic diodicity (the ratio of the pressure drop of the backward flow to the forward flow). The backward flow is the flow in the direction where the flow confronts a higher flow resistance, while the forward flow is the flow in the direction where the flow confronts a lower flow resistance. There are two conventional rectifying geometries commonly studied in the literature: nozzle/diffuser and Tesla geometries (Olsson et al. 1995; Forster et al. 1995). Fadl et al. (2007) experimentally measured the microfluidic diodicity for several nonconventional geometries, and the results suggested that flow rectification might be achievable by using nonconventional geometries other than nozzle/diffuser and Tesla geometries. Recently, Fadl et al. (2009) numerically evaluated the microfluidic diodicity at low Reynolds numbers for both conventional geometries and nonconventional geometries, and the results suggested that there are nonconventional geometries such as the bifurcation geometry which can effectively rectify the flow at low Reynolds number. The work by Fadl et al. (2009) showed that the bifurcation geometry has the highest microfluidic diodicity at low Reynolds numbers among other nonconventional rectifying geometries investigated in the study.

Several studies were published in the literature that focused primarily on valve-less rectification micropumps. Most of the studies have used either Tesla or nozzle/diffuser geometries for flow rectification. For example, Stemme and Stemme (1993), Olsson et al. (1995, 1997b), Gerlach and Wurmus (1995), Gerlach (1997), Jiang et al. (1998), Büttgenbach and Robohm (1999), Singhal et al. (2004), Chen et al. (2008), and Shen and Liu (2008) conducted researches on valve-less rectification micropumps based on nozzle/diffuser geometries. They employed flat-walled and pyramid-trunk-shaped nozzle/diffuser geometries. They also tested micropumps with one chamber versus two chambers. In their studies, a PZT diaphragm was utilized to actuate the micropump, and silicon-glass or polydimethylsiloxane (PDMS)-glass were used to fabricate the micropumps. There were many inconclusive results throughout the literature as discussed by Fadl et al. (2009). However, most results showed that the micropump performance has a strong dependence on the flow Reynolds number and nozzle/diffuser angle. The performance of valve-less rectification micropump has been numerically simulated and characterized by many researchers (Olsson et al. 1997a, 2000; Sun and Huang 2006; Cui et al. 2008). Other studies had also been conducted to characterize the losses within a nozzle/diffuser geometry (Yang et al. 2004; Rosa and Pinho 2006; Wang et al. 2009a).

Similar to the nozzle/diffuser-based micropump research, valve-less rectification micropumps based on the valvular conduits (Tesla's geometry) have been reported in the literature as well. Design, fabrication, and testing of the micropumps were conducted by Forster et al. (1995) and Bardell et al. (1997). Other studies included the transport of particle-laden fluids using valve-less rectification micropumps (Jang et al. 1999), the effect of the particle-laden fluids on the performance of the valve-less rectification micropumps (Jang et al. 2000), optimization (Gamboa et al. 2005), and a low-order modeling of resonance for valve-less rectification micropumps (Morris and Forster 2003) were also conducted in the literature.

According to our literature search, the majority of the valve-less rectification micropumps are based on nozzle/

diffuser and Tesla structures. Both structures work effectively at high frequency. In fact, Gerlach and Wurmus (1995), Olsson et al. (1996), and Koch et al. (1998) (nozzle diffuser) reported that flow rectification is not achievable in laminar flow. Moreover, Gamboa et al. (2005) (Tesla structure) showed in his results that flow rectification is not achievable when Re is less than 200. However, most microbiological applications have fluid flows at low Reynolds number (Geschke et al. 2004). Wang et al. (2009b) have reported an optimized design for a valve-less rectification micropump based on nozzle/diffuser where they examined the pump performance against low actuator frequencies (0–20 Hz). The maximum reported flow rate was 0.06 μl/min. Moreover, valve-less rectification micropumps based on nozzle/diffuser and Tesla structures are unidirectional when no structural modifications are introduced. In this study, we introduce a valve-less rectification micropump that is capable of rectifying the flow at low Reynolds number/low frequency, achieve bidirectional pumping, and multifunctions (pumping and mixing). Additionally, because of the nature of the bifurcation, they can well integrate in microarrays since they can be designed in single and multiple generations. Therefore, the nature design of microarrays by itself can be used to rectify the flow when an oscillating flow is introduced. As a result, the extra pressure drop introduced by external rectifying geometries can be eliminated.

The first bidirectional valve-less rectification micropump was claimed by van der Wijngaart et al. (2000) where maximum flows of +30 μl/min and −30 μl/min were measured. However, the operating frequency were between 0.1 and 80 kHz. Another bidirectional valveless micropump was reported by Hayamizu et al. (2003) where the micropump was controlled by driving waveform. The micropump generated maximum flow rates of +393 nl/s and −323 nl/s in the forward and backward directions, respectively. Moreover, an additional bidirectional valve-less rectification micropump was reported by using two oblique channels and two pump chambers with two PZT actuators (Yoon et al. 2007). The reported flow rate ratio (the ratio between the discharge flow rate and the suction flow rate) was only between 1.01 and 1.03. It is noted that the net flow rate is the difference between the rates of the suction and discharge flows.

Microsystems devices that can combine mixing and pumping work were reported in the literature. Lastochkin et al. (2004) reported a microfluidic pump and mixer based on AC faradaic, Yang et al. (1998) reported the first micropump with active micromixer using turbulence to enhance the mixing of liquids, Rife et al. (2000) miniaturized acousto-fluidic devices to operate a valve-less micropump and produce mixing in low Reynolds number flows, Deshmukh et al. (2001) reported a continuous micromixer with pulsatile flow micropump using silicon on insulator (SOI) and quartz dies and, finally, Sheen et al. (2007) studied the flow characteristics and mixing performance in a PZT self-priming micromixer by using micro-particle-image velocimetry (micro-VIP).

According to our literature review, the only work which employed the bifurcation geometry to rectify the flow was reported exclusively at the macro scale (Jianhui et al. 2007). In this work, the bifurcation geometry was made of a Y-shaped circular tube (which will be difficult to fabricate at the micro scale). The reported maximum flow rate and the mean pressure were 3 ml/min and 33 Pa, respectively.

In this paper, we introduce a novel valve-less rectification micropump based on a bifurcation geometry and PDMS micro fabrication techniques. Three different micropumps based on three different bifurcation configurations were designed, fabricated, and experimentally investigated at a low frequency range. Additionally, we introduce a new dimensionless parameter to evaluate the efficiency of the valve-less rectification micropumps and determine the optimum micropump operational frequency.

2 Pumping mechanism and characterization

Valve-less rectification micropumps are displacement mechanical micropumps and recognized by being valve-less. Instead of having dynamic valves, the valve-less rectification micropumps have rectifying geometries (passive valves) to rectify the flow. The rectifying geometries have flow resistances that depend on the flow direction. The ratio of the pressure drop in both directions is called microfluidic diodicity and it is defined as follows (Forster et al. 1995):

$$D_{\mathrm{i}} = \frac{\Delta P_{\mathrm{b}}}{\Delta P_{\mathrm{f}}}$$

where D_{i}, ΔP_{b}, and ΔP_{f} are the microfluidic diodicity, pressure drop in the backward direction, and pressure drop in the forward direction, respectively. In order to achieve flow rectification, the value of the microfluidic diodicity must be different than one. The efficiency of the flow rectification depends on the value of the microfluidic diodicity. High rectification efficiency means efficient micropump.

To achieve net flow rates through flow rectification, the following two conditions must be met: first, generation of oscillatory flows; second, flow oscillation in rectifying geometries. Typically, PZT actuators are used to generate oscillatory flows, and the rectifying geometries are used to rectify the flows. Nozzle/diffuser and Tesla structures are typical rectifying geometries in the literature. Regardless of the rectifying geometries type, all valve-less rectification

micropumps share the same pumping mechanism and factors that may affect the pumping performance. The parameters that affect the pumping performance are mainly associated with the actuators (PZT) and rectifying geometries. Therefore, the valve-less rectification micropumps can be characterized with respect to the actuator characteristics and the geometrical characteristics of the rectifying geometries. In general, parameters that have an influence on the oscillatory flow behavior will certainly affect the pumping performance to a certain extend.

With respect to the rectifying geometries, the flow resistance coefficients in the forward and backward directions (ξ_f and ξ_b) are employed to characterize the micropumping efficiency (Olsson et al. 1995, 2000; Jiang et al. 1998; Singhal et al. 2004; Yang et al. 2008). In the present design, the backward direction is the direction from the main channel to the secondary channel, while the forward direction is the direction from the secondary channel to the main channel. The forward and backward flow resistance coefficients can be defined as:

$$\xi_f = \frac{\Delta P_f}{\rho V_f^2/2}$$

$$\xi_b = \frac{\Delta P_b}{\rho V_b^2/2}$$

where ξ_f, ξ_b, V_f, V_b, and ρ are the flow resistance coefficients in the forward direction, flow resistance coefficients in the backward direction, flow velocity in the forward direction (secondary channel), flow velocity in the backward direction (main channel), and the fluid density, respectively. The pressure drop along the rectifying geometry is influenced apparently by the geometrical parameters of the rectifying geometries such as nozzle diffuser angle and nozzle diffuser length in the case of the nozzle/diffuser micropump (Olsson et al. 1997a, b, 2000; Yang et al. 2004; Gamboa et al. 2005). In our design, the geometrical parameters may include the bifurcation angle, the width ratio between the main and secondary channels, number of generations, and the symmetry of the secondary channels. The flow resistance coefficient and the time-dependent chamber volume are utilized to calculate the flow rates and pump pressure, respectively, with different arrangement of pump chambers (Ullmann 1998).

In addition to the friction factor, the flow resistance can be predicted by the geometry effects such as conversion and diversion in the case of nozzle/diffuser (Jiang et al 1998; Olsson et al. 1999). The rectifying-directing capability of the rectifying geometries is defined by the ratio of the resistance coefficient in the backward direction to the resistance coefficient in the forward direction as

$$\eta = \frac{\xi_b}{\xi_f}$$

the value of η is larger than one when the net flow rate in the forward direction (as predicted) and smaller than one when a reverse flow in the backward direction may occur.

Besides the flow resistance, the flow inductance needs to be considered to investigate the effects of the unsteady flow on the flow behavior in the valve-less rectification micropumps. The conventional expression given in the literature for the flow impedance is given as follows

$$\hat{Z} = \frac{\Delta \hat{P}}{\hat{Q}} = R + i\omega I$$

where $\hat{Z}$, $\Delta\hat{P}$, $\hat{Q}$, R, ω and I are the complex form of the flow impedance, complex form of pressure drop, volume of flow rate, flow resistance, radian frequency, and fluid inductance, respectively. It shows that impedance is primarily affected by flow resistance and pressure oscillating frequency (Morris and Forster 2003, 2004). In the case of oscillating flow, the velocity is derived based on the time-dependent pressure gradient. Since the pressure gradient is only a function of time and typically expressed in the form of Fourier series or Euler formula, a phase-lag may exist between the flow velocity and the pressure gradient. The synchronization between the flow velocity and the pressure gradient can be identified qualitatively by using Wormersley number (Wo) where it can compare the transient initial force to the viscous force (Loudon and Tordesillas 1998)

$$\mathrm{Wo} = r\sqrt{\frac{n}{v_f}}$$

where r, n, and v_f are characteristic length of channel, radial oscillating frequency, and kinematic viscosity of the fluid, respectively. When $\mathrm{Wo} < 1$ no phase-lag can be observed and the flow velocity synchronize well with the time-dependent pressure gradient. However, this is not the case when Wo is larger than one where phase-lag between the flow velocity and the pressure gradient can be observed. Moreover, when $\mathrm{Wo} = 10$ the parabolic-shape velocity profile is no longer exists when the flow oscillates in circular tubes. The maximum velocity is not located at the center; instead, it is shifted toward the channel wall (Uchida 1956; White 1999).

Reynolds number is a critical parameter that is used widely to characterize the valve-less rectification micropumping (Olsson et al. 1995, 2000; Jiang et al. 1998; Yang et al. 2004; Gamboa et al. 2005; Singhal et al. 2004; Chen et al. 2008; Wang et al. 2009a). However, contradictions over flow rectification with respect to Reynolds number were reported in the literature. For example, some studies suggested that flow rectification in a nozzle/diffuser element is not achievable in laminar flow (Gerlach and Wurmus 1995; Olsson et al. 1996; Koch et al. 1998), while

Singhal et al. (2004) reported that flow rectification is achievable in a nozzle/diffuser element for laminar flow.

PZT actuators play also a role in characterizing the valve-less rectification micropumping. The PZT type, PZT frequency, PZT thickness, PZT excitation signals, PZT driving voltage, and PZT displacement are factors that were reported in the literature to have an influence on the micropumping performance (Stemme and Stemme 1993; Forster et al. 1995; Gerlach and Wurmus 1995; Jang et al. 1999; Morris and Forster 2003; Tracey et al. 2006; Sun and Huang 2006; Cui et al. 2007; Yoon et al. 2007; Cui et al. 2008). Additionally, local and global sharp peaks pumping flows were reported when the PZT actuators reach local and global resonance frequencies, respectively (Park et al. 2002; Feng and Kim 2004).

Additionally, Jianhui et al. (2007) have predicted the flow rate and mean pressure of valve-less rectification pump in the macro scale based on bifurcation geometry. In their work, they showed analytically that the pumping characteristics depend on the characteristics of the rectifying geometry, flow field, and PZT like other pumps in their category. However, their work was in the mini scale and the bifurcation was fabricated in circular tubes.

Finally, air bubbles were reported in the literature to have a negative effect on the micropumping performance of the valve-less rectification micropumps (Richter et al. 1998; Shen and Lu 2008). To summarize, all valve-less rectification micropumps have the same pumping principles, but differ in the type of the rectifying geometries. Many factors have an effect on the pumping performance of the valve-less rectification micropumps, and they are divided into two categories: first, parameters that are related to the rectifying geometry and, secondly, parameters that are related to the pumping actuators. The presence of bubbles is found to have a negative effect on the pumping performance of the valve-less rectification micropumps.

3 The micropump design

Computer-aided design software (AutoCAD, Autodesk Inc., San Rafael, CA, USA) was used to design the desired bifurcation rectifying configurations. Three different bifurcation designs were employed: a single bifurcation, a double-generation bifurcation, and a hybrid bifurcation design (combined micromixer and micropump applications), as shown in Fig. 2.

The first design, a single bifurcation shown in panel (a) of Fig. 2 was intended to be used as a benchmark design as well as to prove the feasibility of the valve-less rectification micropump based on the bifurcation rectification geometry. The second design is the double-generation bifurcation shown in panel (b), which was intended to compare its micropumping performance to the micropumping performance of the single generation design (to investigate the effect of the number of generations). Both designs, single and double-generation configurations have one inlet and one outlet. In contrast, the third design shown in panel (c) of Fig. 2 was intended to investigate the capacity of a multifunction microfluidic device and to integrate a micromixer and micropump into one single design. The third design has two inlets and one outlet which is one of the advantages of using the bifurcation geometry to rectify the flow in a micropump. Because of the inherent nature of the bifurcation geometry (one main channel and two secondary channels), it was feasible to pump and mix two different fluids using a single microfluidic device.

The diameters of the micropump chamber and PZT are 10 and 12 mm, respectively. The first design has two secondary channels, while the second design has two secondary and four sub-secondary channels. The height of the channels is 230 μm, and the width ratio of the channels before and after the bifurcating tip is 2. In other words, the width of the main channel is twice the width of the secondary channel. Similarly, the width of the secondary channel is twice the width of the sub-secondary channel, in the case of the double generation design. All the secondary channels have the same width, as do the sub-secondary channels. The width of the main channel is 200 μm and the bifurcation angle is 90° (the angle between the secondary channels as well as the sub-secondary channels). In the case of the first and second design, the width of the collecting chamber is 2.5 mm (the chamber located between the bifurcation geometry and the inlet/outlet channels). On the other hand, the diameter of the inlet/outlet circle, in the case of the third design, is 2 mm. Guides or aligning structures (the structures that can be seen around the micropump chamber in Fig. 2) were implemented in the designs to better align the PZT actuators during the fabrication process. The arrows in Fig. 2 refer to the predicted pumping direction.

4 Fabrication procedure

The bidirectional and multifunction valve-less rectification micropump consists of five components: channels, a pump chamber, a membrane, an actuator, and a sealer. The membrane, the micropump channels, and the pump chamber were fabricated using PDMS Replica Molding (REM). The PZT (Digi-Key Corp., Thief River Falls, MN, USA) was used to actuate the micropump, and soda-lime glass substrates were used to seal the channels and the pump chambers.

The softlithography technique was employed as the main fabrication method; see Fig. 3 for the fabrication steps. First, a glass wafer was cleaned and dehydrated on a hotplate at a temperature of 120°C for 1 h (step 1). Second,

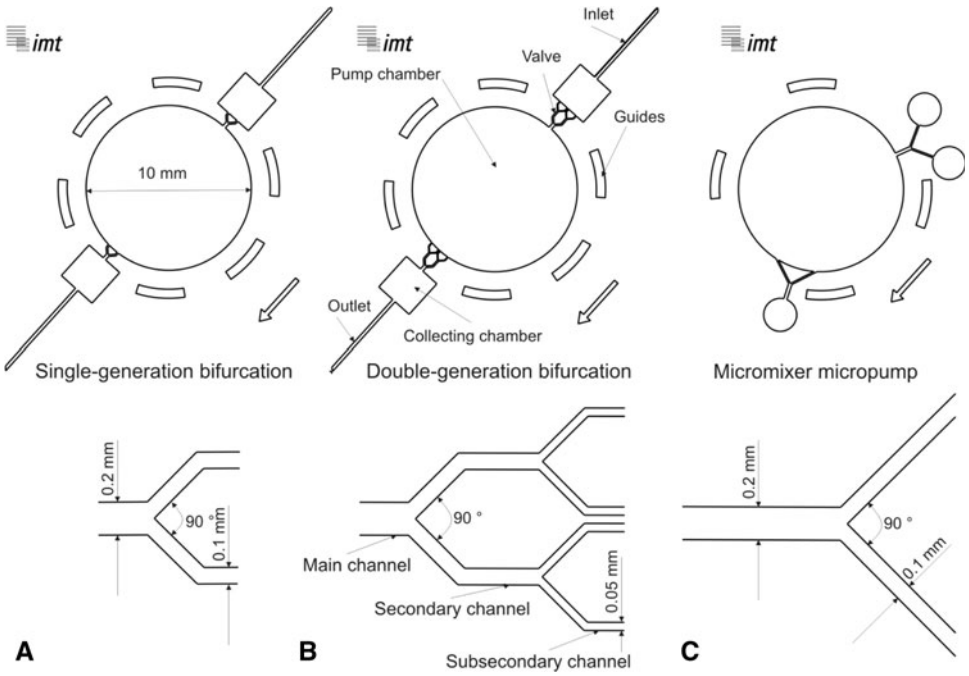

Fig. 2 Bifurcation designs implemented in the present investigation: **a** single bifurcation; **b** double-generation bifurcation; **c** hybrid bifurcation

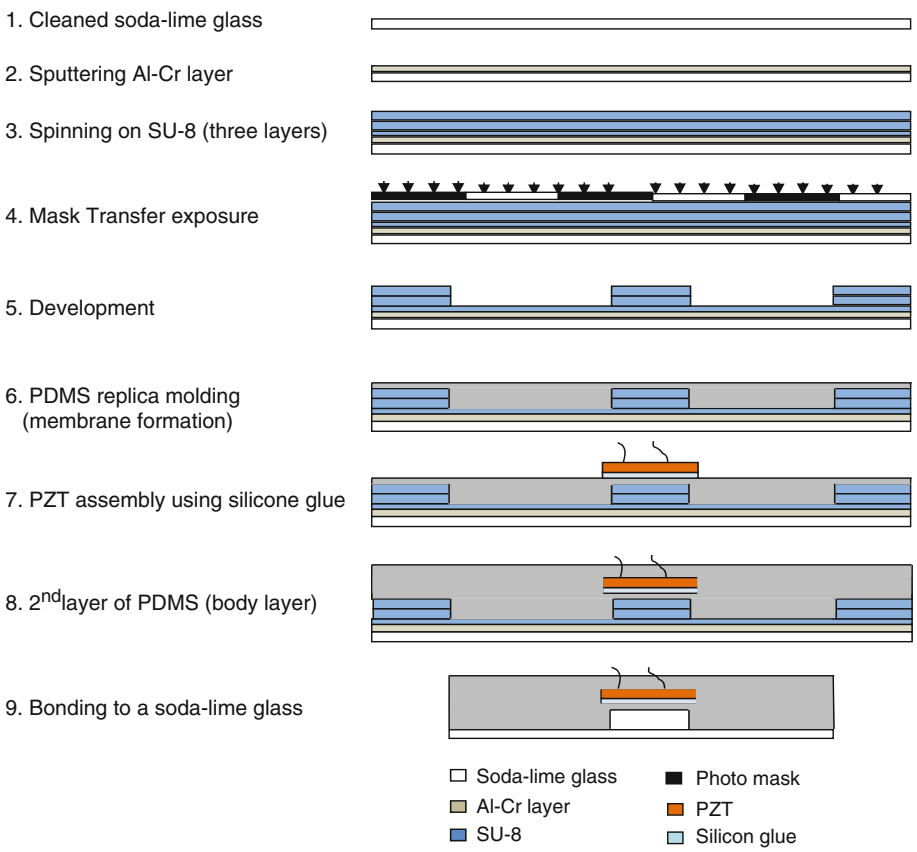

Fig. 3 The fabrication procedure of the valve-less rectification micropumps based on bifurcation geometry

a thin layer of chromium (10 nm) was sputtered on the glass wafer to achieve better adhesion (step 2). Thirdly, three layers, base and two structure layers, of an epoxy-based negative photoresist (SU-8, MicroChem Corp., Newton, MA, USA) were spun on using a spinning machine. The first layer was 5 μm thick (SU8-5) and acted as an adhesion promoter. The second and third layers were created as structure layers with a total thickness of 230 μm

(step 3). The wafer was then exposed to UV-light for cross linking (step 4). The first fabrication step ends with developing the master wafer in γ-butyrolactone (GBL) and propylene glycol methyl ether acetate (PGMA, MicroChem Corp., Newton, MA, USA) (step 5). The master wafer was then inspected under the microscope and extra development time was given when needed. The master wafer was then inspected to assure a uniform thickness by using an advanced surface texture measuring system (Dektak8, Veeco Instruments Inc., Tucson, AZ, USA).

The second step included fabricating the channels, pump chamber, membrane, and integrating the actuator (PZT). The PDMS (Sylgard 184 elastomer kit, Dow Corning, Midland, MI, USA) was mixed at a ratio of 10:1 (silicon elastomer base:curing agent). The mixture was degassed under vacuum until all trapped air bubbles were released. The double sided moulding (Lucas et al. 2008) was used to precisely produce a 200 μm thick membrane (step 6). After the curing of the PDMS membrane layer, a small droplet of silicon glue (RS Components, Mörfelden-Walldorf, Germany) was placed on the bottom of the PZT and then the PZT was pushed against the membrane (step 7). At the same time, a new PDMS mixture was prepared and degassed. The new mixture was poured on the wafer and placed on the hot plate (step 8). After the PDMS was cured, the PDMS-PZT was peeled off carefully and slowly.

The third fabrication step included bonding the PDMS-PZT composite to a lime-soda glass wafer. First, the lime-soda glass was diced and cleaned using water, acetone, and ethanol, respectively. The glass and PDMS-PZT were placed inside a barrel etcher (Surface Technology Systems, Newport, UK). As a result, an irreversible bond was formed due to the surface treatment in an oxygen plasma environment (step 9). Finally, the fabrication procedure ended with fluidic connections of metallic micropipes at the inlets and outlets.

5 Experimental apparatus

Figure 4 shows the experimental apparatus which was used in the present investigation. The experimental apparatus consists of an amplifier (E-508.00 HVPZT, PI Physik Instrumente, Karlsruhe, Germany), a frequency generator (Agilent 33220A, Agilent Technologies Deutschland GmbH, Böblingen, Germany), an oscilloscope (Tektronix, Japan), a digital microscopic camera (dnt Gmbh, Dietzenbach, Germany), and a laptop. A square signal and 220 V with a zero offset were used to control the PZT. The choice of the excitation signal was based on the fact that the square signal is the typical exciting signal in microfluidic micropumps (Jang et al. 2009). Indeed, Forster et al. (1995) reported that the output of fixed-valve micropumps was significantly larger for the square signal than the sinusoidal signal. The micropump was investigated against two ranges of actuator frequencies, 0–100 Hz and 0–300 Hz, the first range has small increments (5 Hz) and was chosen to test flow rectification at low frequency and to observe the changes in the flow rectification behavior when small increments were chosen. The second range was chosen to investigate the flow rectification when larger increments (50 Hz) were utilized. The second range is large enough to accommodate the 50 Hz increments and keep the fluid flow in the laminar region (the Reynolds number for the oscillating flow in the main channel is around 2000 when the PZT actuator's frequency is equal to 300 Hz). In general, the choice of the actuator frequencies is arbitrary and it was reported to be between 0.1 and 5000 Hz (Laser and Santiago 2004). Typically, water, methanol, and ethanol were utilized as working fluids in mechanical micropumps (Laser and Santiago 2004). Since PDMS is hydrophobic (exhibit slip boundary condition; Byun et al. 2008) and methanol is toxic, ethanol was used as a working fluid in all the experiments. Flow rate measurements were conducted based on the bubble tracking method (Yoon et al. 2007; Wang et al. 2009b) in the inlet/outlet tube. To evaluate the flow rate measurement errors, the flow rate was measured using two different methods at two different locations, simultaneously. In the inlet tube, an air bubble was trapped and the bubble velocity between two specified marks was measured using a stopwatch. At the same time, the discharged fluid was collected from the outlet tube during the same time when the bubble moved between the two marks. The discharged fluid was weighed on a scale (Scout Pro

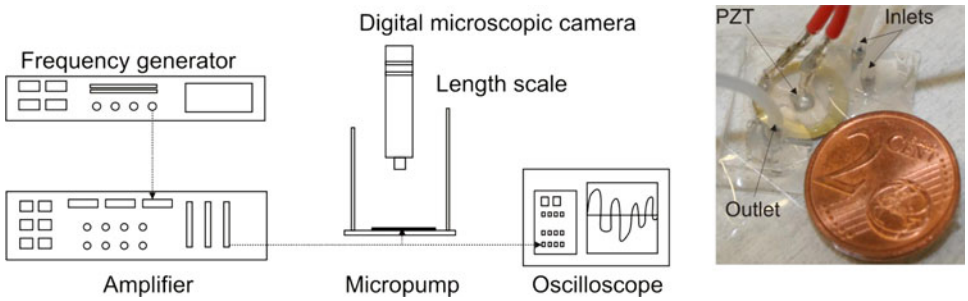

Fig. 4 The experimental apparatus; the hybrid bifurcation micropump

SPU402, OHAUS Corp., Pine Brook, NJ, USA), and the mass used to calculate the flow rate. The difference in the flow rate values between the two measurement methods was less than 3%. To evaluate the experimental error, experimental samples were randomly chosen and repeated three times. The error analysis suggested that the experimental error is equal to or less than 10% with a confidence interval of 90%.

A length scale (ruler) was attached to the experimental stand for back pressure measurements (ethanol column height). The digital microscopic camera was fixed under the micropump chamber to monitor the flow in real time during the experiments. The real-time monitoring of the flow behavior during the experiments provided assistance to analyze the experimental data. A blue dye (Pelikan, Hannover, Germany) was used in the experiments to better visualize the flow behavior and clearly track the position of the air bubble inside the inlet/outlet tubes. The frequency and the voltage were monitored during the experiments by using an oscilloscope.

6 Pump efficiency

In the micropump literature, researchers have typically characterized the micropump performance by the micropump flow rate and back pressure. Pump flow rate and back pressure are important parameters for pumps of any scale. However, it is noted that the use of the flow rate and back pressure alone to characterize micropumps is not sufficient. For example, power consumption should be a vital parameter to evaluate micropumps. Therefore, the efficiency of the micropumps plays a crucial rule when an evaluation process is considered. Valve-less rectification micropumps were fabricated in different methods (e.g. soft lithography and hard lithography); employed different actuators (e.g. pneumatic and PZT actuators), membranes (e.g. PDMS and silicone), and rectification geometries (e.g. Tesla and nozzle/diffuser); tested at different resonance frequencies and voltages; and, not surprisingly, the micropumps delivered different flow rates and back pressures. Valve-less rectification micropumps rectify an oscillating flow to a one way flow. Therefore, it has two different flow velocities: one is the mean oscillating fluid velocity and the other is the net unidirectional flow velocity. The latter is the velocity difference between the forward and backward flow, which can be observed at the inlet/outlet tube. Thus, only a fraction of the input energy through the actuator can be effectively utilized to generate the net unidirectional flows. The input power E' (J/s) utilized to pump the fluid in a channel can be calculated as $E' = \Delta F V$, where ΔF is the total force difference across the channel and V is the average fluid velocity. For oscillation flows inside the chamber, the average velocity V_0 can be estimated as $V_0 = 2hf$, where h is the membrane deflection and f is the PZT frequency. Typically, the piezoelectric actuators have relatively small strains on the order of 0.1% (Mulling et al. 2001); therefore, the deflection can be approximated using the following formula:

$$h = 0.001 * D_{\mathrm{PZT}} \tag{1}$$

where D_{PZT} is the diameter of the PZT. In other words, the membrane deflection, approximately, is equal to 0.1% of the PZT diameter. Assuming the difference in ΔF inside the chamber and at the inlet/outlet can be neglected, the ratio of the average fluid velocities in the pump chamber and the inlet/outlet tube can be used as a third parameter to better assess the valve-less rectification micropumps efficiency and locate the optimum operational frequency where the maximum flow rate per each pumping cycle is delivered. It is true that neglecting the force difference is quite arbitrary in the above discussion, a better characterization of the valve-less rectification micropumps efficiency is open for discussions. The following formula was used to evaluate the dimensionless parameter which was employed to evaluate the efficiency of the valve-less rectification micropumps as well as locating the optimal operational frequency:

$$\text{Efficiency} = \frac{E'_{\mathrm{out}}}{E'_{\mathrm{in}}} \sim \bar{V} = \frac{V_{\mathrm{net}}}{V_0} \tag{2}$$

where $E'_{\mathrm{out}}, E'_{\mathrm{in}}, \bar{V}, V_0,$ and V_{net} are the output power, input power, dimensionless parameter (the velocity ratio), average velocity inside the micropump chamber, and the average unidirectional velocity inside the inlet/outlet tubes, respectively.

7 Results and discussion

Three bifurcation designs were tested and the results are presented in four different diagrams: flow rate versus frequency (0–100 Hz), flow rate versus frequency (0–300 Hz), flow Reynolds number versus frequency, and velocity ratio versus frequency.

Figure 5 shows a comparison in the results between the single and double-bifurcation micropumps. Panel (a), the flow rate versus frequency diagram in the frequency range of 0–100 Hz, with small increments of 5 Hz, shows that rectification is achievable at all frequencies between 0 and 100 Hz. Additionally, a bidirectional pumping was observed in this frequency range of the experiments where the flow reverses the direction in the frequency range between 25 and 40 Hz. The maximum positive and negative flow rates are 8 and 10.5 μl/min, respectively. The positive flow is the flow in the predicted direction as shown in Fig. 2, while the negative flow is the flow in the opposite

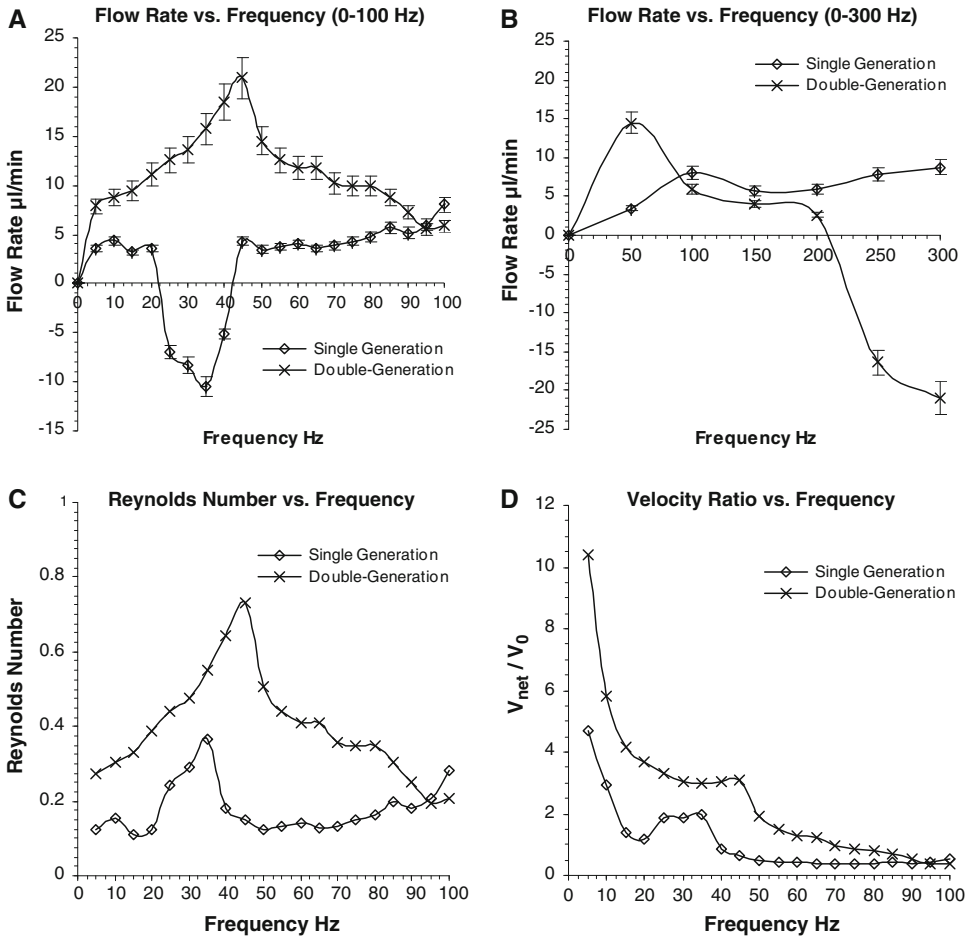

Fig. 5 The results of the single- and double-generation bifurcation designs. **a** Flow rate versus frequency (0–100 Hz); **b** flow rate versus frequency (0–300 Hz); **c** Reynolds number versus frequency; **d** velocity ratio versus frequency

direction. While the double-generation result shows that flow rectification is achievable at all frequencies. However, the phenomenon of bidirectional pumping was not observed at the frequency range of 25–40 Hz as shown in the single bifurcation micropump design. The maximum positive flow rate is 20.94 µl/min occurring at $f = 45$ Hz. Panel (b) is the flow rate versus frequency in the oscillation frequency range of 0–300 Hz with increments of 50 Hz. Panel (b) shows that the phenomenon of bidirectional pumping (reversing the flow direction) is not observable when a large increment is employed in the case of the single generation design; and the flow rate increased and reached a local peak at 100 Hz and then decreased and reached a local minimum between the frequency of 150 and 200 Hz. After 200 Hz, the flow rate is increasing monotonically as the frequency increases. The maximum flow rate of 8.7 µl/min was observed at 300 Hz. On the other hand, the double-generation result shows that the phenomenon of bidirectional pumping is observable when the frequency is increased beyond 200 Hz. The flow reverses direction and a negative flow rate was observed at 250 and 300 Hz. The maximum negative flow rate was 20.94 µl/min at 300 Hz, which is the same value as the maximum positive flow rate that occurs at $f = 45$ Hz as shown in panel (a). Panel (c) displays the Reynolds number versus frequency. In the case of the single generation design, the Reynolds number diagram shows that the Reynolds number in the inlet/outlet tube ranges between 0.12 and 0.36. Corresponding to panel (a), the flow Reynolds number reaches the maximum at the frequency of 35 Hz. In contrast, Reynolds number in the inlet/outlet tube in the case of the double-generation design is between 0.1 and 0.73, bearing the same patterns displayed in panel (a). The velocity ratio versus the PZT frequency is displayed in panel (d) of Fig. 5. The pump efficiency can be estimated based on the value of the velocity ratio. Results show that the optimum frequency (maximum velocity ratio) occurs when the frequency is equal to 5 Hz for both designs, single and double generations. At this frequency, the losses in the flow energy were minimized, and the maximum flow rate per each pumping cycle is delivered. The maximum value of the velocity ratio is 4.71 and 10.41 in the case of single- and double-generation designs, respectively. Furthermore, the maximum back pressure in the case of the single generation design is 0.46 kPa when $f = 35$ Hz and the flow rate = 0 µl/min. Whereas the maximum back

pressure in the case of the double-generation design is 1.0 kPa when $f = 45$ Hz and the flow rate = 0 μl/min.

Figure 6 shows the experimental results for the third design of the bifurcation configuration which is intended for the combined micromixing-micropumping applications. Panel (a), the flow rate versus frequency, in the frequency range of 0–100 Hz with small increments of 5 Hz, shows again that rectification is achievable at all frequencies. However, the phenomenon of bidirectional pumping is not observable. The zigzag flow rate pattern as a function of the frequency has three minimums and three peaks. The three minimums occur at 15, 35, and 80 Hz and the three peaks occur at 20, 65, and 95 Hz, respectively. The measured maximum positive flow rate is 137 μl/min. In panel (b), the flow rate versus frequency between 0 and 300 Hz, with increments of 50 Hz, the results show that the phenomenon of bidirectional pumping is also not observable in the entire range of frequencies under investigation, which is different from the experimental findings with respect to the first and second designs. The flow rate increased monotonically with the actuator frequency. The maximum positive flow rate is observed at $f = 300$ Hz and equal to 116 μl/min. Panel (c), the Reynolds number versus frequency, shows that the Reynolds number varies between 0.36 and 2.4 in the frequency between 0 and 100 Hz. Panel (d), the velocity ratio versus frequency, shows that the optimum operational frequency (maximum velocity ratio) is $f = 5$ Hz. At this frequency, the maximum velocity ratio is 23.25 while the maximum back pressure is 2.86 kPa when $f = 90$ Hz and the flow rate = 0 μl/min.

Experimental results in Fig. 5 show that the double-generation bifurcation micropump design performed better than the single generation bifurcation design. The double-generation design has a higher flow rate as well as maximum back pressure. It is also noted that the capability of bidirectional pumping was observed at different actuator frequencies. The bidirectional pumping phenomenon was observed at a low frequency range for the single bifurcation design, while for the double-generation bifurcation design, it occurs at relatively high frequencies (250 and 300 Hz). Two explanations can be given to justify that the bidirectional pumping phenomenon occurs at two different ranges of actuator frequencies. First, the microfluidic diodicity is not equal for both designs. That means, for a specific frequency each design will confront a different ratio of flow resistance. Second, the single generation design would

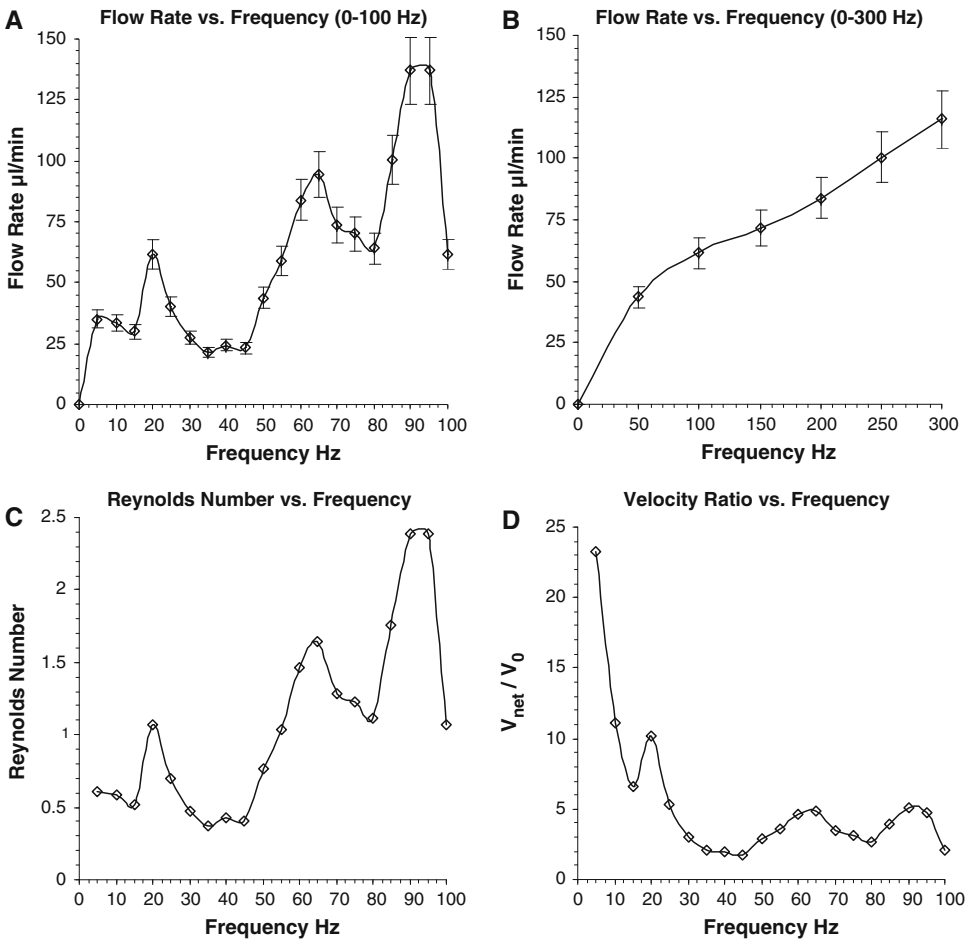

Fig. 6 The results of the hybrid bifurcation design. **a** Flow rate versus frequency (0–100 Hz); **b** flow rate versus frequency (0–300 Hz); **c** Reynolds number versus frequency; **d** velocity ratio versus frequency

tolerate larger size air bubbles than the double-generation design (the width of sub-secondary tubes in the double-generation design is half the width of the secondary tubes in the single generation design). Thus, the sub-secondary channels in the second design may become blocked by air bubbles that can often pass through the secondary channels, in the first design, due to the difference in channel width between both designs. As a result, an extra deviation in the microfluidic diodicity between both designs would be introduced. Both explanations may suggest that it would be difficult for the bidirectional phenomenon to occur at the same actuator frequency for the two different designs with different values of microfluidic diodicity.

In contradiction to the single-generation and double-generation designs, the hybrid-bifurcation design (for the combined micromixing-micropumping applications) did not exhibit any bidirectional pumping capability. Both the first and second designs have fluid collecting chambers. The existence of these collecting chambers has added additional losses (entrance and exit losses) to the fluid flow. As a result, using the microfluidic diodicity of the bifurcation geometry by itself without taking into consideration the collecting chamber will result in prediction errors. For example, using numerical simulations to predict the experimental results or to determine the rectification efficiency of the micropump based on the microfluidic diodicity of the rectifying geometry alone will not be accurate, since the rectification characteristics of the micropump are entirely dependent on the total microfluidic diodicity which includes the bifurcation geometry as well as the collecting chamber.

Using numerical simulations, Fadl et al. (2009) predicted that the microfluidic diodicity of the bifurcation geometry will increase with the increase of the flow Reynolds number or actuator frequency. As a result, the net flow rate, theoretically, will increase monotonically with the Reynolds number/actuator frequency. However, in practice, many factors affect the characteristics of micropump performance. For example, due to the PDMS permeation of gas, the flow is two-phase instead of a single-phase flow (most numerical simulations and theoretical analysis treat the flow as a single phase flow). Additionally, gas permeation through the PDMS walls may lead to a slip boundary condition (Singh et al. 1998; Randall and Doyle 2005; Huang et al. 2006; Tremblay et al. 2006; Sadrzadeh et al. 2009). Air bubbles were clearly visible in the experiments, and they have certainly significant effects on the flow dynamics. It was also observed that the bubbles' size inside the micropump vary with the actuator frequency as shown in Fig. 7. Figure 7 also shows that the size of air bubbles increases as frequencies increase from $f = 10$ to $f = 80$ Hz. This is valid for both designs (single generation and double-generation). Moreover, the way the air bubbles interact with the rectifying geometries has a significant effect on the rectification characteristics. Depending on the bubbles size, the bubbles may pass through the rectifying geometry or stagnate at the entrance of the rectifying geometry. As a result, the value of the microfluidic diodicity would be changed and the outcome would be hard to predict. We believe that the combined effects of extra losses caused by the collecting chamber, permeation properties of the PDMS, dynamics of bubble interactions in the two-phase flow with the rectifying geometries, as well as the possible deformation of the PDMS structures under the oscillatory pressure variations, have changed the

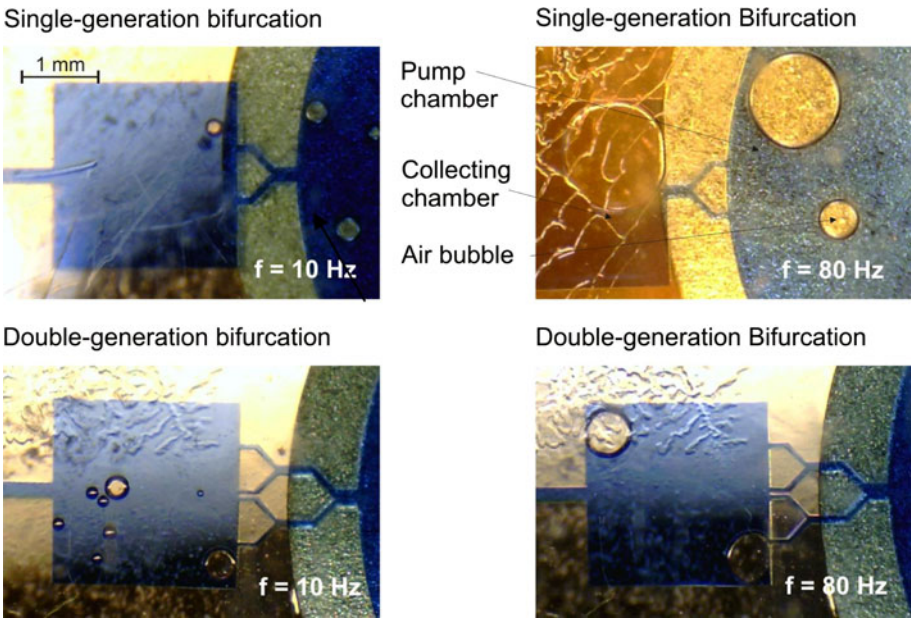

Fig. 7 Air bubbles inside the pump and collecting chambers in the case of the single generation and double-generation designs (notice the difference in the bubble size when the frequency increases from 10 to 80 Hz)

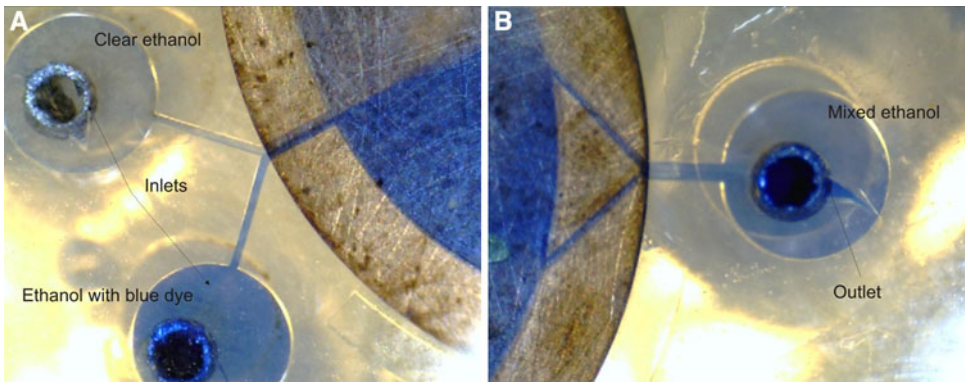

Fig. 8 The micromixer-micropump based microfluidic device. Parallel flow layers are visible at the inlets and a mixing was visually observed at the outlet

characteristics of the microfluidic diodicity and, as a result, triggered the bidirectional pumping phenomena. Predictions and simulations of these interactions are challenging and are out of the scope of the current investigation.

The third design, the hybrid-bifurcation configuration for combined micromixing-micropumping applications, shows some promising results. It has the highest flow rate, back pressure, and velocity ratio among the three designs. It has no collecting chamber as needed in the other two designs. As a result, no extra losses were introduced and the trend of microfluidic diodicity predicted by computer simulation was not disturbed. The microfluidic diodicity of the bifurcation geometry itself dominates the total diodicity of the micropump. The absence of the collecting chamber has aided the air bubbles to pass through the channels instead of being trapped in the collecting chamber. Additionally, the missing of the introduced losses caused by the collecting chamber has normalized the microfluidic diodicity to be only correlated to the bifurcation geometry. This may explain why the bidirectional pumping phenomenon was not observed in the hybrid design.

The proposed micropump efficiency is related to the flow rates delivered by each pumping cycle (supply mode and pump mode; see Fig. 1). Therefore, it is feasible to locate the actuator frequency where the flow rate per each pumping cycle is maximized. The results show that the maximum flow rate per each pumping cycle is occurred at 5 Hz for all three designs. However, the maximum total flow rates are delivered at different actuator frequencies for all three designs. For example, the maximum total flow rate for the first design is 10.47 μl/min at 35 Hz which reflects 0.29 μl/min per each pumping cycle. While the flow rate is 3.56 μl/min at 5 Hz which reflects 0.71 μl/min per each pumping cycle. Similarly, the flow rate per each pumping cycle at the maximum total flow rates are 0.46 and 1.4 μl/min, while the flow rates per each pumping cycle are 1.57 and 3.5 at 5 Hz for the second and third designs, respectively. Therefore, the velocity ratio may be used to evaluate the micropump performance beside other conventional parameters (total flow rate and maximum back pressure).

The multi-functionality of mixing and pumping was demonstrated in the experiments. The mixing was examined at different frequencies and visually observed at the micropump outlet. However, micromixing in Y-channel was reported by Kim et al. (2003) and Yi and Bau (2003). Panel (a) in Fig. 8 shows the photo of two streams of ethanol at the inlets. A clear ethanol was introduced to one inlet and an inked ethanol to the second one. Parallel layers were clearly visible at the inlet region and mixing was visually observed at the outlet region as shown in panel (b). The experiment shown in Fig. 8 was conducted at $f = 60$ Hz. However, a further investigation is required to quantify the mixing performance of the hybrid design, and it is out of scope of the current work.

Finally, all three bifurcation-based micropump designs are proven to be self-priming. They are capable of pumping liquids and gases as well. To test the self-priming capability, the micropump was activated when the entire micropump was filled with air. Subsequently, a liquid flow was established and observed through the micropump and a net flow rate was detected at the outlet tube. When comparing the results with the results reported by Wang et al. (2009b), the valve-less rectification micropup based on the bifurcation geometry has delivered higher flow rate at the same frequency and voltage than the valve-less rectification micropump based on the nozzle/diffuser in the low actuator frequency region. Wang et al. (2009b) has reported 0.06 μl/min at 10 Hz and 200 V, while our third design, hybrid design, delivered 33.5 μl/min at 10 Hz and 220 V. However, this comparison may not be accurate due to differences in the micropump design and experimental parameters such as rectifying geometries, PZT type, PZT diameter, and excitation signal.

8 Conclusions

Three different valve-less rectification micropumps based on bifurcation geometry were designed, fabricated, and tested. All three micropumps are self-priming. The

bidirectional pumping capabilities were demonstrated at certain actuator frequencies for the single bifurcation and the double-generation bifurcation micropumps, while the multi-functionality of micromixing-micropumping was demonstrated for the hybrid bifurcation design. While the double-generation bifurcation design shows better results than the single-bifurcation design, the hybrid bifurcation design was associated with the highest flow rate (137 μl/min), maximum back pressure (2.86 kPa), and pump efficiency (23.25). A non-dimensional group was introduced as a third parameter associated with the pump efficiency, in addition to the flow rate and maximum back pressure, to better evaluate the performance and determine the optimum operational frequency of the valve-less rectification micropumps where the maximum flow rate per each pumping cycle is delivered. Additionally, increasing the actuator frequency with small increments (5 Hz) led to observations of the bidirectional pumping phenomena in the first design. This phenomenon has not been observed when the large increments (50 Hz) were considered. The results also suggest that the highest pumping efficiency occurs at the lowest actuator frequency.

In practice, many factors affect the characteristics of valve-less rectification micropumps and the prediction and simulation of these factors are challenging and need further investigation.

Acknowledgment The research described in this paper was supported by the National Science Foundation (NSF), grant no.: OISE-0530203.

References

Amirouche F, Zhou Y, Johnson T (2009) Current micropump technologies and their biomedical applications. Microsyst Technol 15:647–666

Bardell R, Sharma R, Forster FK, Afromowitz MA, Penney R (1997) Designing high-performance micro-pumps based on no-moving-parts valves. In: Lin L, Goodson KE et al (eds) Microelectromechanical systems (MEMS), Proceedings of the ASME IMECE (International Mechanical Engineering Congress and Exposition), vol DSC-234/HTD-354. Dallas, pp 47–53

Büttgenbach S, Robohm C (1999) Microflow devices for miniaturized chemical analysis systems. Proc SPIE 3539:51–61

Byun D, Jihoon K, Ko HS, Park HC (2008) Direct measurement of slip flows in superhydrophobic microchannels with transverse grooves. Phys Fluids 20(11):113601–13601-9

Chen Y, Kang S, Wu L, Lee S (2008) Fabrication and investigation of PDMS micro-diffuser/nozzle. J Mater Process Technol 198:478–484

Cui Q, Liu C, Zha XF (2007) Study on a piezoelectric micropump for the controlled drug delivery system. Microfluid Nanofluid 3:377–390

Cui Q, Liu C, Zha XF (2008) Simulation and optimization of a piezoelectric micropump for medical applications. Int J Manuf Technol 36:516–524

Deshmukh AA, Liepmann D, Pisano AP, Lee LP (2001) Continuous microfluidic mixing using pulsatile micropumps. Ph.D. dissertation, Berkeley Sensor and Actuator Center, University of California, Berkeley, CA, USA

Fadl A, Zhang Z, Faghri M, Meyer D, Simmon E (2007) Experimental investigation of geometric effect on microfluidic diodicity. Proceeding of the fifth International conference on microchannels and minichannels ICNMM2007-30074, June 18–20, 2007, Puebla, Mexico

Fadl A, Zhang Z, Geller S, Tölke J, Krafczyk M, Meyer D (2009) The effect of the microfluidic diodicity on the efficiency of valve-less rectification micropumps using Lattice Boltzmann Method. Microsyst Technol 15:1379–1387

Feng G-H, Kim ES (2004) Micropump based on PZT unimorph and one-way parylene valves. J Micromech Microeng 14:429–435

Forster FK, Bardell L, Afromowitz MA, Sharma NR, Blanchard A (1995) Design, fabrication and testing of fixed-valve micropumps. Proc ASME Fluids Eng Div ASME 234:39–44

Gamboa AR, Morris CJ, Forster F (2005) Improvements in fixed-valve micropump performance through shape optimization of valves. J Fluid Eng 127:339–346

Gerlach T (1997) Pumping gases by a silicon micro pump with dynamic passive valves. International conference on solid-state sensors and actuators, Chicago, June 16–19, 1997, Tranceducers'97-2A3.03

Gerlach T, Wurmus H (1995) Working principles and performance of the dynamic micropump. Sens Actuators A 50:135–140

Geschke O, Klank H, Tellemann P (2004) Microsystem engineering of lab-on-a-chip devices. Wiley-VCH Verlag GmbH & Co. KGaA, Weinheim

Hayamizu S, Higashino K, Fujii Y, Sando Y, Yamamoto K (2003) Development of a bi-directional valve-less silicon micro pump controlled by driving waveform. Sens Actuators A 103(1–2):83–87

Huang P, Guasto JS, Breuer KS (2006) Direct measurement of slip velocities using three-dimensional total internal reflection velocimetry. J Fluid Mech 566:447–464

Iverson B, Garimella S (2008) Recent advances in microscale pumping technologies: a review and evaluation. Microfluid Nanofluid 5:145–174

Jang LS, Morris C, Sharma N, Bardell R, Forster F (1999) Transport of particle-laden fluids through fixed-valve micropumps. Microelectromechanical systems (MEMS)-ASME 1999, MEMS, vol 1

Jang LS, Sharma N, Forster F (2000) The effect of particles on performance of fixed-valve micropumps. Micro Totao Anal Syst 283–286

Jang L-S, Kan W-H, Chen M-K, Chou Y-M (2009) Parameter extraction from BVD electrical model of PZT actuator of micropumps using time-domain measurement technique. Microfluid Nanofluid 7:559–568

Jiang XN, Zhou ZY, Huang XY, Li Y, Yang Y, Liu CY (1998) Micronozzle/diffuser flow and its application in microvalveless pumps. Sens Actuators A 70:81–87

Jianhui Z, Jizhuang L, Qixiao X (2007) Research on the valveless piezoelectric pump with Y-shape pipes. Front Mech Eng China 2(2):144–151

Kim MC, Kim S, Park JS, Park HD (2003) Numerical simulation of micromixing pulsatile micropump. J Ind Eng Chem 9(5):602–606

Koch T, Evans AGR, Brunschweiler A (1998) The dynamic micropump driven with screen printed PZT actuator. J Micromech Microeng 8:119–122

Laser DJ, Santiago JG (2004) A review of micropumps. J Micromech Microeng 14:35–64

Lastochkin D, Zhou R, Wang P, Ben Y, Chang H-C (2004) Electrokinetic micropump and micromixer design based on ac faradic polarization. J Appl Phys 96:1730–1733

Loudon C, Tordesillas A (1998) The use of the dimensionless Womersley number to characterize the unsteady nature of internal flow. J Theor Biol 191:63–78

Lucas N, Demming S, Jordan A, Sichler P, Büttgenbach S (2008) An improved method for doublesided moulding of PDMS. J Micromech Microeng 18:1–5

Morris CJ, Forster FK (2003) Low-order modeling of resonance for fixed-valve micropumps based on first principles. J Microelectromech Syst 12(3):325–334

Morris CJ, Forster FK (2004) Oscillatory flow in microchannels-comparison of exact and approximate impedance models with experiments. Exp Fluids 36:928–937

Mulling J, Usher T, Dessent B, Palmer J, Franzon P, Grant E, Kingon A (2001) Load characterization of high displacement piezoelectric actuators with various end conditions. Sens Actuators A 94:19–24

Nguyen N, Huang X, Chuan TK (2002) MEMS-micropumps: a review. J Fluid Eng 124:384–392

Olsson A, Stemme G, Stemme E (1995) A valve-less planar fluid pump with two pump chambers. Sens Actuators A 46–47:549–556

Olsson A, Stemme G, Stemme E (1996) Diffuser-element design investigation for valve-less pumps. Sens Actuators A 57:137–143

Olsson A, Stemme G, Stemme E (1997a) Simulation studies of diffuser and nozzle elements for valve-less micropumps. Transducers 97, June 16–19, Chicago, USA

Olsson A, Enoksson P, Stemme G, Stemme E (1997b) Micromachined flat-walled valve-less diffuser pumps. J Microelectromech Syst 6(2):161–166

Olsson A, Stemme G, Stemme E (1999) A numerical design study of the valveless diffuser pump using a lumped-mass model. J Micromech Microeng 9:34–44

Olsson A, Stemme G, Stemme E (2000) Numerical and experimental studies of flat-walled diffuser elements for valve-less micropumps. Sens Actuators 84:165–175

Park J-H, Yokota S, Yoshida K (2002) A piezoelectric micropump using resonance drive with high power density. JSME Int J 45(2):502–509

Randall GC, Doyle PS (2005) Permeation-driven flow in poly(dimethylsiloxane) microfluidic devices. Proc Natl Acad Sci USA 102(31):10813–10818

Richter M, Linnemann R, Woias P (1998) Robust design of gas and liquid micropumps. Sens Actuators 68:480–486

Rife JC, Bell MI, Horwitz JS, Kabler MN, Auyeung RCY, Kim WJ (2000) Miniature valveless ultrasonic pumps and mixers. Sens Actuators A 86:135–140

Rosa S, Pinho FT (2006) Pressure drop coefficient of laminar Newtonian flow in axisymmetric diffusers. Int J Heat Fluid Flow 27:319–328

Sadrzadeh M, Amirilargani M, Shahidi K, Mohammadi T (2009) Gas permeation through a synthesized composite PDMS/PES membrane. J Memb Sci 342:236–250

Sheen HJ, Hsu CJ, Wu TH, Chu HC, Chang CC, Lei U (2007) Experimental study of flow characteristics and mixing performance in a PZT self-pumping micromixer. Sens Actuators A 139:237–244

Shen C-Y, Liu H-K (2008) Fabrication and drive test of piezoelectric PDMS valveless micro pump. J Chin Inst Eng 31(4):615–623

Singh A, Freeman BD, Pinnau I (1998) Pure and mixed gas acetone/nitrogen permeation properties of polydimethylsiloxane [PDMS]. J Polym Sci B Polym Phys 36:289–301

Singhal V, Garimella SV, Murthy J (2004) Low Reynolds number flow through nozzle-diffuser elements in valveless micropumps. Sens Actuators A 113:226–235

Stemme E, Stemme G (1993) A valve-less diffuser/nozzle based fluid pump. Sens Actuators A 39:159–167

Sun CL, Huang K (2006) Numerical characterization of the flow rectification of dynamic microdiffusers. J Micromech Microeng 16:1331–1339

Tracey MC, Johnston ID, Davis JB, Tan CKL (2006) Dual independent displacement-amplified micropumps with a single actuator. J Micromech Microeng 16:1444–1452

Tremblay P, Savard M, Vermette J, Paquin R (2006) Gas permeability, diffusivity and solubility of nitrogen, helium, methane, carbon dioxide and formaldehyde in dense polymeric membranes using a new on-line permeation apparatus. J Membr Sci 282:245–256

Uchida S (1956) The pulsating viscous flow superposed on the steady laminar motion of incompressible fluid in a circular pipe. ZAMP 7:403–422

Ullmann A (1998) The piezoelectric valve-less pump-performance enhancement analysis. Sens Actuators A 69:97–105

van der Wijngaart W, Andersson H, Enoksson P, Noren K, Stemme G (2000) The first self-priming and bi-directional valve-less diffuser micropump for both liquid and gas. MEMS 2000, 23–27 Jan 2000, Miyazaki, Japan, pp 674–679

Wang Y, Hsu J, Kuo P, Lee Y (2009a) Loss characterization and flow rectification property of diffuser valves for micropumps application. Int J Heat Mass Transf 52:328–336

Wang C-T, Leu T-S, Sun J-M (2009b) Optimal design and operation for a No-Moving-Parts-Valve (NMPV) micro pump with a diffuser width of 500 μm. Sensors 9:3666–3678

White FM (1999) Fluid mechanics. WCB/McGraw-Hill, Singapore

Yamahata C, Vandevyver C, Lacharme F, Izewska P, Vogel H, Freitag R, Gijs M (2005) Pumping of mammalian cells with a nozzle-diffuser micropump. Lap on a Chip 15:1083–1088

Yang Z, Goto H, Matsumoto M, Yada T (1998) Micromixer incorporated with piezoelectrically driven valveless micropump, Micro Total Analysis Systems '98. Kluwer Academic Publishers, Dordrecht, pp 177–180

Yang K, Chen I, Shew B, Wang C (2004) Investigation of the flow characteristics within a micronozzle/diffuser. J Micromech Microeng 14:26–31

Yang H, Tsai T-H, Hu C-C (2008) Portable valve-less peristaltic micropump design and fabrication. DTIP of MEMS & MOEMS, 9–11 April, French Riviera, France

Yi M, Bau HH (2003) The kinematics of bend-induced mixing in micro-conduits. Int J Heat Fluid Flow 24:645–656

Yoon J, Choi J, Lee H, Kim M (2007) A valveless micropump for bidirectional applications. Sensors Actuators A 135:833–838